Two-Dimensional Inert Accumulation in Space Hydrogen-Oxygen Fuel Cells

R. W. LYCZKOWSKI and DIMITRI GIDASPOW

IIT Center
Institute of Gas Technology, Chicago, Illinois 60616

Fuel cell compartments are of two types: through-flow and dead-ended. Dead-ended anode and cathode compartments are used when pure reactants are available, such as hydrogen and oxygen in space vehicles. Gases enter the compartment only upon load demand due to a reduction in pressure in the cavity. But even ultrapure fuels and oxidants have some impurities which accumulate and cause a drop in voltage due to dilution of the reactants. In Part I of this study (*1*) we obtained concentration profiles as a function of time for the case when the flow in the fuel cell can be considered one-dimensional. We also suggested a method of improved operation of a fuel cell involving bleeding of inerts. This was based on the observation that the inerts accumulate near the dead end of the cell.

The assumption of one-dimensionality of flow and diffusion in an actual fuel cell must, however, be questioned. This is due to the fact that the inlet ports are made quite small. The size of the opening, for example, in some of Allis-Chalmers cells, is about 1 mil in diameter as compared with a cell width of 4 in. In the one-dimensional model, the inlet port corresponds to the full 4-in. width. In the present two-dimensional model, the ports can be point sources or have any desired width.

In the one-dimensional model (*1, 2*) it was possible to obtain the solution for the buildup of inerts by considering only the reacting species equation and the continuity equation. The flow field was obtained by simple quadrature of the current density. For the two-dimensional problem, we have to consider the fluid mechanics in the fuel cell cavities. The flow would be simply creeping motion, called Hele-Shaw flow, were it possible to have empty cavities, since the Reynolds number is small (*2*). However, structural rigidity, desirability to have current collectors contacting the electrodes, and the necessity to remove heat by conduction apparently led Allis-Chalmers to build the gas compartments with a complex internal structure. In an earlier study (*3, 4*), it was shown that the flow field can be successfully described by the use of Darcy's law. Two empirical permeabilities were determined for a typical Allis-Chalmers flow configuration, one for the basic direction of flow and the other for the perpendicular direction. Using these values, theoretical pressure curves based on the solution of the resulting Laplace's equation for pressure were verified experimentally using an actual Allis-Chalmers fuel cell compartment (*5*). The agreement was such that we can safely use this model to describe our fluid mechanics in a dead-ended cell operated under load, with bleed or even during the purge operation.

Correspondence concerning this article should be addressed to Professor Dimitri Gidaspow. R. W. Lyszkowski is with Goodyear Atomic Corporation, Piketon, Ohio.

MATHEMATICAL MODEL

Consider a thin rectangular cavity into which a gas containing a small amount of impurity enters through a small opening (Figure 1). The gas reacts electrochemically on one side of the surfaces and disappears. The contaminant remains in the cavity and acts as a dilutant. The product water of the electrochemical reaction either leaves through the electrochemical face or is removed in the other chamber through a water removal plaque and is not important in this analysis.

In Figure 1 the chamber is taken to be h thick, and for this development, all properties are considered to be averaged in the direction perpendicular to the electrode surface. The conservation of reacting gas a is given in weight units by (after the usual limiting procedures)

$$\epsilon \frac{\partial \rho_a}{\partial t} + \frac{\partial}{\partial x}(\rho_a q_{ax}) + \frac{\partial}{\partial y}(\rho_a q_{ay}) = -\frac{IM_a}{hnF} \qquad (1)$$

which states mathematically the scheme

(rate of accumulation of a)
+ (net rate out by convection of a)
= rate of generation of a in the element Δx by Δy

q_{ax} and q_{ay} are the seepage velocity components of species a.

When the term main or basic direction of flow is used in our discussion, it will refer to the x direction, because this is the principal direction of flow and is also the one-dimensional direction of flow.

A similar equation is written for species b and added to Equation (1). This yields the continuity equation which is written for the purpose of the analysis to follow as

$$\rho\left(\frac{\partial q_x}{\partial x} + \frac{\partial q_y}{\partial y}\right) = -\frac{IM_a}{hnF} - \epsilon\frac{\partial \rho}{\partial t} - q_x\frac{\partial \rho}{\partial x} - q_y\frac{\partial \rho}{\partial y} \qquad (2)$$

We now perform an order of magnitude analysis. Introduce the dimensionless variables, ad hoc

$$p = \frac{Pg_c}{\rho^0 U^2} \qquad N^0{}_{Re} = \frac{hU\rho^0}{\mu}$$

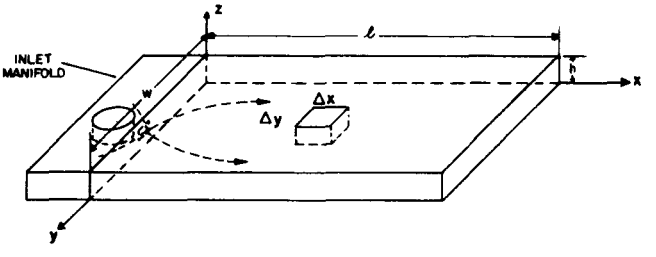

Fig. 1. Fuel cell chamber geometry.

$$\bar{q}_x = \frac{q_x}{U} \qquad \bar{x} = \frac{x}{l}$$

$$\bar{q}_y = \frac{q_y}{U} \qquad \bar{y} = \frac{y}{w}$$

$$\bar{\rho} = \frac{\rho}{\rho^0} \qquad \theta = \frac{tU}{h\epsilon}$$

$$\bar{I} = \frac{IM_a}{h\, nF\, \rho^{0^2}\, \mu\, U^2} \tag{3}$$

which transform Equation (2) into

$$\bar{\rho}\left[\left(\frac{h}{l}\right)\frac{\partial \bar{q}_x}{\partial \bar{x}} + \left(\frac{h}{w}\right)\frac{\partial \bar{q}_y}{\partial \bar{y}}\right] = N^0{}_{Re}\left[-\bar{I} + \left(\frac{k_x}{l^2}\right)\frac{\partial p}{\partial \bar{x}}\cdot\frac{\partial \bar{\rho}}{\partial \bar{x}} + \left(\frac{k_y}{w^2}\right)\frac{\partial p}{\partial \bar{y}}\cdot\frac{\partial \bar{\rho}}{\partial \bar{y}} - \frac{\partial \bar{\rho}}{\partial \theta}\right] \tag{4}$$

Since k_x and k_y are of the order of h^2 or less and the dimensionless partials are of the order one, the terms involving (k_x/l^2) and (k_y/w^2) may be dropped with respect to the other terms on the right-hand side of Equation (4) to yield

$$\rho\left(\frac{\partial q_x}{\partial x} + \frac{\partial q_y}{\partial y}\right) = -\frac{IM_a}{hnF} - \epsilon\frac{\partial \rho}{\partial t} \tag{5}$$

which constitutes the simplified continuity equation.

Darcy's law is

$$q_x = -\frac{k_x g_c}{\mu}\frac{\partial P}{\partial x} \tag{6}$$

and

$$q_y = -\frac{k_y g_c}{\mu}\frac{\partial P}{\partial y} \tag{7}$$

where P already stands for the perturbation pressure in the cavity. The inlet pressure is maintained constant, so that only small differences in pressure produce the driving force for motion.

Since $\rho = C_a M_a + C_b M_b + C_{H_2O} M_{H_2O}$ and we know that C, the total molar concentration, is constant for an ideal gas under isothermal conditions, we obtain $d\rho = dC_A \cdot (M_A - M_B)$. We may then write

$$\frac{\partial \rho}{\partial t} = \frac{\partial \rho}{\partial C_a}\frac{\partial C_a}{\partial t} = (M_a - M_b)\frac{\partial C_a}{\partial t} \tag{8}$$

Use of Darcy's law, together with Equation (8), transforms the continuity equation, Equation (5), into

$$k_x\frac{\partial^2 P}{\partial x^2} + k_y\frac{\partial^2 P}{\partial y^2} = \frac{\mu}{g_c}\left[\frac{IM_a}{hnF\rho} + \frac{\epsilon}{\rho}(M_a - M_b)\frac{\partial C_a}{\partial t}\right] \tag{9}$$

It is easy to show, using the dimensionless groups, that the accumulation may be neglected to within an order of magnitude of a few percent as compared to the load if the time is scaled by the experiment time. This is typically of the order of an hour or more. Therefore, we drop the unsteady terms in both Equations (5) and (9).

The use of Fick's law of diffusion

$$\rho_a q_{ax} = \rho_a q_x - \epsilon_x D_{ab}\frac{\partial \rho_a}{\partial x} \tag{10}$$

$$\rho_a q_{ay} = \rho_a q_y - \epsilon_y D_{ab}\frac{\partial \rho_a}{\partial y} \tag{11}$$

in the steady form of the simplified continuity equation causes the species a equation to assume the form

$$\epsilon\frac{\partial \rho_a}{\partial t} + \frac{IM_a}{hnF}\left(1 - \frac{\rho_a}{\rho}\right) + q_x\frac{\partial \rho_a}{\partial x} + q_y\frac{\partial \rho_a}{\partial y} = D_{ab}\left(\epsilon_x\frac{\partial^2 \rho_a}{\partial x^2} + \epsilon_y\frac{\partial^2 \rho_a}{\partial y^2}\right) \tag{12}$$

ϵ_x and ϵ_y act as sort of tortuosity factors to account for the circuitous paths of diffusion in the web-type cavity. They can be related to ratios of open areas in the two directions of flow.

Use of the two easily derived relations which relate the molar and weight-averaged seepage velocities for constant total molar concentration C

$$q_x{}^* = q_x - \epsilon_x\frac{D_{ab}}{\rho}(M_a - M_b)\frac{\partial C_a}{\partial x} \tag{13}$$

$$q_y{}^* = q_y - \epsilon_y\frac{D_{ab}}{\rho}(M_a - M_b)\frac{\partial C_a}{\partial y} \tag{14}$$

in Equation (12) results in

$$\epsilon\frac{\partial \rho_a}{\partial t} + \frac{IM_a}{hnF}\left(1 - \frac{\rho_a}{\rho}\right) + q_x{}^*\frac{\partial \rho_a}{\partial x} + q_y{}^*\frac{\partial \rho_a}{\partial y} = D_{ab}\left(\epsilon_x\frac{\partial^2 \rho_a}{\partial x^2} + \epsilon_y\frac{\partial^2 \rho_a}{\partial y^2}\right) + \frac{M_a D_{ab}(M_a - M_b)}{\rho}\left[\left(\frac{\partial C_a}{\partial x}\right)^2 + \left(\frac{\partial C_a}{\partial y}\right)^2\right] \tag{15}$$

We now drop the square of the partial derivatives with respect to x and y, as is the accepted practice, for example, see reference 6. This is reasonable although not necessary for our method of solution in view of the following situation.

It was seen in the one-dimensional model that the derivative of the concentration was primarily changing only across a blurred front. Near the entrance port, C_a is constant and so the derivative is nearly zero. Past the front, the inert has accumulated and thus the derivative of C_a is again zero. Therefore the molar and weight-averaged seepage velocities differ only across this front at different times. In addition, the $2 - D$ effect is largely a correction to the more desirable $1 - D$ flow, and the $1 - D$ model is exact. Therefore, since the effect is fairly localized, we will write, from Equations (13) and (14)

$$q_x{}^* = q_x \quad \text{and} \quad q_y{}^* = q_y \tag{16}$$

If $M_a = M_b$, then Equation (16) is exact as seen from Equations (13) and (14).

The final form of the equations we concern ourselves with is

Species equation:

$$\epsilon\frac{\partial x_a}{\partial t} + \frac{(1 - x_a)\, IM_a}{hnF\rho} + q_x{}^*\frac{\partial x_a}{\partial x} + q_y{}^*\frac{\partial x_a}{\partial y} = D_{ab}\left(\epsilon_x\frac{\partial^2 x_a}{\partial x^2} + \epsilon_y\frac{\partial^2 x_a}{\partial y^2}\right) \tag{17}$$

Continuity equation:

$$k_x\frac{\partial^2 P}{\partial x^2} + k_y\frac{\partial^2 P}{\partial y^2} = \frac{I\mu}{g_c\, hnFC} \tag{18}$$

Velocity components (Darcy's law):

$$q_x = q_x{}^* = -\frac{k_x g_c}{\mu}\frac{\partial P}{\partial x} \tag{19}$$

$$q_y = q_y^* = -\frac{k_y g_c}{\mu}\frac{\partial P}{\partial y} \tag{20}$$

DIMENSIONLESS EQUATIONS AND BOUNDARY CONDITIONS

Thus, for the case of nearly constant density, the introduction of the dimensionless variables transforms Equations (17) to (20) into

Species equation:

$$\frac{\partial x_a}{\partial \theta} + (1 - x_a)\psi + \bar{q}_x^* \frac{\partial x_a}{\partial \bar{x}} + \bar{q}_y^* \frac{\partial x_a}{\partial \bar{y}} = D^* \left(\frac{\partial^2 x_a}{\partial \bar{x}^2} + \frac{\epsilon_y}{\epsilon_x} \frac{\partial^2 x_a}{\partial \bar{y}^2} \right) \tag{21}$$

Continuity equation:

$$\frac{\partial^2 \bar{P}}{\partial \bar{x}^2} + \left(\frac{k_y}{k_x}\right) \frac{\partial^2 \bar{P}}{\partial \bar{y}^2} = \psi \tag{22}$$

Velocity components (Darcy's law):

$$\bar{q}_x = \bar{q}_x^* = -\frac{\partial \bar{P}}{\partial \bar{x}} \tag{23}$$

$$\bar{q}_y = \bar{q}_y^* = -\left(\frac{k_y}{k_x}\right) \frac{\partial \bar{P}}{\partial \bar{y}} \tag{24}$$

The same set of equations applies for the purge cycle or bleed as well, because the average velocities are still very low. The only modifications that are necessary are in the boundary conditions.

The set of boundary conditions that we now consider represents the point-source problem with a specified reactant purity at the pinhole opening and dead-ended operation. The species equation boundary conditions are as follows:

$$x_a(0, \bar{x}, \bar{y}) = x_a^i(\bar{x}, \bar{y})$$

$$\frac{\partial x_a}{\partial \bar{y}}(\theta, \bar{x}, 0) = \frac{\partial x_a}{\partial \bar{y}}(\theta, \bar{x}, \gamma) = 0$$

$$\frac{\partial x_a}{\partial \bar{x}}(\theta, 1, \bar{y}) = 0; \; x_a(\theta, 0, \bar{y}') = x_a^0(\theta)$$

$$\frac{\partial x_a}{\partial \bar{x}}(\theta, 0, \bar{y}) = 0, \text{ except at } (0, \bar{y}') \tag{25}$$

where $\bar{y}'$ is the position of the pinhole opening and $\gamma = w/l$.

At the pinhole opening $(0, \bar{y}')$ in the dead-ended cell, there is a point source of unknown pressure strength Q. Everywhere else, $\partial \bar{P}/\partial n = 0$, where n is an outward-drawn normal. In the next two sections we drop the bars over the dimensionless independent variables for convenience.

METHOD OF SOLUTION

The system of partial differential equations to be solved closely resembles that encountered in the solution of the complete incompressible two-dimensional Navier Stokes equations (7). Our diffusion equation, Equation (21), corresponds to the vorticity transfer equation. Our continuity equation for the pressure corresponds to the equation for the stream function. In both cases the velocity components are obtained by differentiating the solution obtained from the Poisson's equation, Equation (22). This means that in both cases we have to have intermediate results correct to a considerably larger number of significant figures than the final answers in order not to lose all accuracy in the numerical differentiation. In part due to this difficulty solutions of the Navier-Stokes equations are known to require of the order of 10 hr. on fastest computers. To avoid this expense, we decided to solve our Poisson's equation analytically using Green's functions.

The solution of the nonhomogeneous Laplace's equation, Poisson's equation, Equation (22), can be written using Green's function theory (3, 8) as

$$\bar{P}(x, y; 0, y') = \underset{\text{source}}{Q \cdot G(x, y; 0, y')} - \underset{\text{sink}}{\int_0^1 \int_0^\gamma \psi(x'', y'') \cdot G(x, y; x'' y'')\, dx''\, dy''} \tag{26}$$

Conservation of mass requires that the inlet mass be equal to the consumption, which gives

$$Q = \int_0^1 \int_0^\gamma \psi(x'', y'')\, dx''\, dy'' \tag{27}$$

The Green's function used previously (3) was reduced to single-sum expressions. It may be written as

$$G(x, y; x', y'; x'', y'') = G_{\text{source}}(x, y; x', y') - G_{\text{sink}}(x, y; x'', y'') \tag{28}$$

where

$$G_{\text{source}}(x, y; x', y') = \begin{cases} \frac{1}{\gamma}\left\{\frac{1}{2}(x^2 + x'^2) - x + \frac{1}{3} + \frac{2}{a}\sum_1^\infty \frac{\cos(mby)\cos(mby')\cosh[am(1-x)]\cosh(amx')}{m\sinh(am)}\right\} & (1 \geq x \geq x') \\ \frac{1}{\gamma}\left\{\frac{1}{2}(x^2 + x'^2) - x' + \frac{1}{3} + \frac{2}{a}\sum_1^\infty \frac{\cos(mby)\cos(mby')\cosh[am(1-x')]\cosh(amx)}{m\sinh(am)}\right\} & (x' \geq x \geq 0) \end{cases} \tag{29}$$

$G_{\text{sink}}(x', y'; x'', y'')$ is identical to $G_{\text{source}}(x, y; x', y')$ except that (x'', y'') replaces (x', y') everywhere in Equation (29). It will be noted that the single primes denote the source coordinates and the double primes denote the sink coordinates and bars have been dropped over x and y.

We start operation of the fuel cell with a uniform composition. For a given current density, such as for the dimensionless current density Q/γ equal to 1, we can obtain an analytical solution for the pressure distribution. In the next section we call this distribution corresponding to zero

time $\overline{P}^0$. Then knowing $\overline{P}^0$ we can obtain the velocity components from Darcy's law, Equations (23) and (24).

To obtain the concentration distribution at some later time we use these velocity components in the diffusion equation. We finite difference Equation (21) using a two-dimensional analog of the computational scheme given in Part 1 (*1*). We again satisfy the sufficient stability conditions of Keller (*9*). Having obtained the concentration distribution at some later small increment of time, we calculate the current distribution using the same polarization information and path of operation as in Part I.

For this new non-uniform ψ in Equation (22) we must calculate the new pressure distribution. Since $\psi(x, y)$ is known only as an array of numbers, it is fit to a bilinear expression in each of the number of subregions of the rectangle $(1 \times \gamma)$ as shown in Figure 2. A coarser grid $\Delta x'$ by $\Delta y'$ is superimposed on the finer grids Δx by Δy of $\psi(x, y)$ and $\psi^{ij}(x, y)$ is fit in each of the indicated regions.

The approximation used for $\psi(x, y)$ in each rectangular region is (*10*)

$$\psi^{ij}(x, y) = A^{ij} + B^{ij}\,x + C^{ij}\,y + D^{ij}\,xy \qquad (30)$$

where

$$A^{ij} = \frac{x_{i-1}\,y_{j-1}}{\Delta x'\,\Delta y'}\,(\psi_{i,j} - \psi_{i-1,j} - \psi_{i,j-1} + \psi_{i-1,j-1}) + \psi_{i-1,j-1}\left(1 + \frac{x_{i-1}}{\Delta x'} + \frac{y_{j-1}}{\Delta y'}\right) - \frac{x_{i-1}}{\Delta x'}\,\psi_{i,j-1} - \frac{y_{j-1}}{\Delta y'}\,\psi_{i-1,j} \qquad (31)$$

$$B^{ij} = (\psi_{i,j-1} - \psi_{i-1,j-1})\left(\frac{1}{\Delta x'} + \frac{y_{j-1}}{\Delta x'\,\Delta y'}\right) + \frac{y_{j-1}}{\Delta x'\,\Delta y'}\,(\psi_{i-1,j} - \psi_{i,j}) \qquad (32)$$

$$C^{ij} = (\psi_{i-1,j} - \psi_{i,j-1})\cdot\left(\frac{1}{\Delta y'} + \frac{x_{i-1}}{\Delta x'\,\Delta y'}\right) + \frac{x_{i-1}}{\Delta x'\,\Delta y'}\,(\psi_{i,j-1} - \psi_{i,j}) \qquad (33)$$

$$D^{ij} = (\psi_{i-1,j-1} - \psi_{i,j-1} - \psi_{i-1,j} + \psi_{ij})/\Delta x'\,\Delta y' \qquad (34)$$

and the subscripts denote evaluation of the generation function at their indicated values. The values of x and y are represented by x_{i-1}, x_i, y_{j-1}, and y_j at which points ψ is known; i ranges from 1 to MX where $MX = 1/\Delta x'$ and j ranges from 1 to NY where $NY = \gamma/\Delta y'$. The range of validity for ψ^{ij} is $x_{i-1} \leq x \leq x_i$, $y_{j-1} \leq y \leq y_j$.

The pressure at the point (x, y) due to a source at $(0, y')$ can be represented in the form

$$\overline{P}(x, y; 0, y') = \frac{Q}{\gamma}\cdot\overline{P}^0(x, y; 0, y') - \overline{P}^1(x, y) \qquad (35)$$

and the velocity components as

$$\overline{q}_x = \frac{Q}{\gamma}\,\overline{q}_x^0(x, y; 0, y') + \frac{\partial \overline{P}^1}{\partial x}(x, y) \qquad (36)$$

and

$$\overline{q}_y = \frac{Q}{\gamma}\,\overline{q}_y^0(x, y; 0, y') + \frac{k_y\,\partial \overline{P}^1}{k_x\,\partial y}(x, y) \qquad (37)$$

The partial derivatives were approximated by three-point Newton's forward or backward difference interpolation formulas which are accurate to Δx^2 and Δy^2. We note that the source discontinuity in pressure occurs only in P^0 for which an analytical expression is given in the next section. Thus P^1 and its derivatives are analytic functions. The complete expression for the pressure is given in the Appendix. Details of computation and a computer program are given in Lyczkowski's thesis (*2*).

UNIFORM CURRENT DISTRIBUTION

Uniform current density occurs in a fuel cell if a power load is applied to a fresh module which has an initially uniform reactant gas composition. We may transform the pressure problem with uniform current density generation in a fuel cell chamber into a simpler problem. Let $\overline{P} = u + x^2/2$. This transforms the nonhomogeneous Laplace equation into the homogeneous one (Figure 3). This transform leaves three sides at zero flux and one side, $(x = 1)$, at a uniform negative unit flux. The significance of this unit flux is as follows. As far as the pressure distribution is concerned, the effect of consuming the mass electrochemically over the entire electrode area may be simulated by removing the same quantity of mass at constant flux along the entire width of the dead end of the fuel cell. In either case, the amount of material entering through the pinhole opening must equal the amount leaving. The practical application is as follows. Measurements made of the pressure distribution in a thin rectangular chamber that has a pinhole opening at one end and only a constant mass removal at the other may be used to calculate the pressure distribution in the same chamber with uniform mass removal, either electrochemically or physically, through one or more faces perpendicular to flow.

The solution for the u problem (right side of Figure 3) is simple, because only a single line integral need be performed. Therefore

$$u(x, y; 0, y) = \gamma\cdot G_{\text{source}}(x, y; 0, y') + \int_\Gamma \frac{\partial u}{\partial n}\,\Big|_\Gamma\, G_{\text{sink}}(x, y; \Gamma')\,d\Gamma' \qquad (38)$$

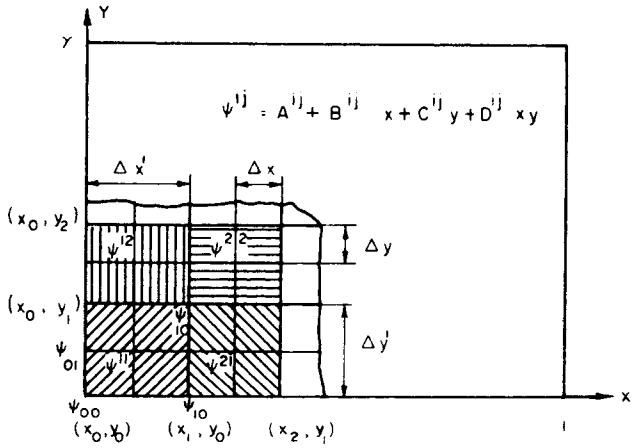

Fig. 2. Geometry for approximating ψ in subregions of the rectangle $(1 \times \gamma)$.

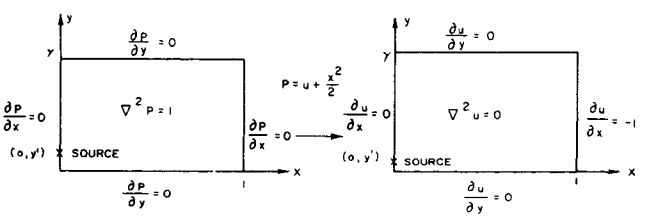

Fig. 3. Conversion of the uniform current generation problem to the constant mass flux removal problem for pressure distribution.

where Γ is the boundary contour and n is the outward drawn normal. For the situation shown in Figure 3

$$u(x, y; 0, y') = \gamma \cdot G_{\text{source}}(x, y; 0, y') - \int_0^\gamma G_{\text{sink}}(x, y; 1, y'')dy'' \quad (39)$$

The integral yields $x^2/2 - 1/6$ so that the result for $\bar{P}^0$ is the same as obtained below except for an additional added constant of 1/6. This added constant makes the perturbation pressure zero at the dead end of the cell at zero time. The absolute value of P is not unique; however differences in pressure needed in this study are unique.

The pressure distribution for unit dimensionless current density, $Q/\gamma = 1$, can also be obtained by integration of Equation (26) using the Green's function given by Equation (29). The result suitable for computation is as follows:

$$\bar{P}^0 = \frac{1}{2}(1-x)^2 - \frac{1}{6} - \frac{1}{2a}\sum_0^N \ln\left[(1 - 2e^{-ax_n}\cos[b(y-y')] + e^{-2ax_n}) \times (1 - 2e^{-ax_n}\cos[b(y+y')] + e^{-ax_n})\right] \quad (40)$$

The velocity components are

$$\bar{q}_x^0 = 1 - x + \frac{1}{2}\sum_0^N (-1)^n \left[\frac{1}{\coth(ax_n) - \dfrac{\cos[b(y-y')]}{\sinh(ax_n)}} + \frac{1}{\coth(ax_n) - \dfrac{\cos[b(y+y')]}{\sinh(ax_n)}}\right] - (-1)^n \quad (41)$$

$$2 > x > 0$$
$$\gamma \geqq y \geqq 0$$

and

$$\bar{q}_y^0 = \frac{1}{2}\sum_0^N \left[\frac{\sin[b(y+y')]}{\cosh(ax_n) - \cos[b(y+y')]} + \frac{\sin[b(y-y')]}{\cosh(ax_n) - \cos[b(y-y')]}\right] \cdot \left(\frac{k_y}{k_x}\right)^{1/2}$$

and where

$$x_0 = x \qquad x_1 = 2 - x \text{ and}$$
$$x_{2n} = x_{2n-1} + 2x \qquad n = 1, 2, \ldots \quad (42)$$
$$x_{2n+1} = x_{2n} + 2 - 2x \qquad n = 1, 2, \ldots$$

N is chosen so that the n^{th} term differs from the term before it by some small quantity ϵ which may be made arbitrarily small, for instance 10^{-20}. It was found that for realistic situations, $N = 1$, in general, so that Equations (40) (41), and (42) are closed-form approximate solutions to the problem.

Two runs were made: $\gamma = 1.0$, $k_x/k_y = 1.0$, and $y' = 0.5$; and $\gamma = 0.60$, $k_y/k_x = 8.1$, and $y' = \gamma/4$. The first run represents Hele-Shaw flow and illustrates the most two-dimensional case possible; the second case approximates the Allis-Chalmers oxygen chamber (*11*).

The dimensionless zero time perturbation pressure P^0 is plotted in Figure 4. Only one-half of the cell is shown, the left half, since symmetry is present about $\bar{y} = 0.5$. The fact that the pressure $\bar{P}$ is positive or negative means that the total pressure is either above or below 36.7 lb./sq. in. abs. In this figure and all the rest, the dead-ended part of the cell is at the top and the entrance port at the bottom. Near the source, circles are obtained for constant $\bar{P}^0$. Circles represent the solution to the problem of a continuous point source in an infinite medium. Near the dead end, straight lines indicate that this part is one-dimensional.

Figures 5 and 6 are plots of constant x and y direction seepage velocity components. In Figure 7 we plot the speed. This type of plot shows that the fastest flowing fluid is near the source, and that stagnation occurs in the corners and near the dead end. A stream function will exist only if we equate the species velocities to the bulk velocities at every point, as done in a related problem by Winsel (*12, 13*). This is true only when diffusion is negligible.

Typical results for the Allis-Chalmers (*11*) fuel cell configuration are shown for pressure and speed in Figures 8 and 9. When one compares the pressure lines of Figures 4 and 8, it becomes obvious that the second figure exhibits far more one-dimensionality than the first. In addition, since the permeability ratio is no longer unity, ellipses result near the source with the longer axis in the direction of the larger permeability. Since the source is off center, the speed lines have become much more complicated as evidenced by comparing Figures 7 and 9. A very small area of slow-moving fluid is to the left of the source, and a larger area is to the right of the source. Beyond $\bar{x} = 0.4$, the cell is essentially one-dimensional.

CHECKS AND BALANCES

After all these approximations and operations we must have some numerical checks. One of the most important

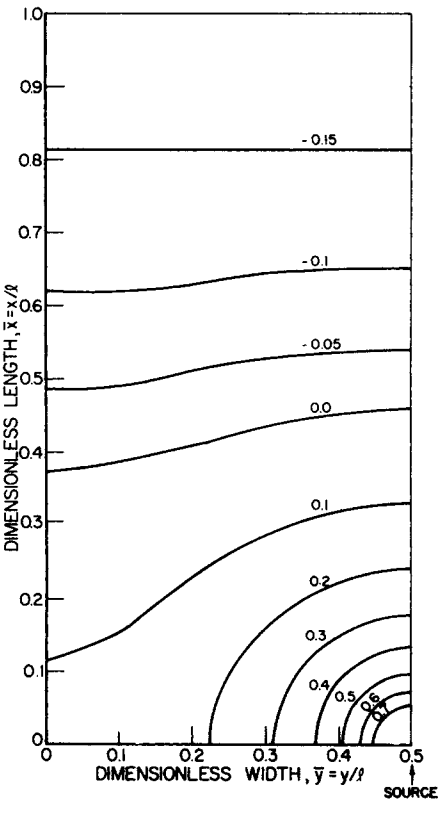

Fig. 4. Lines of constant dimensionless perturbation pressure P^0 at zero time ($\gamma = 1.0$, $k_x = k_y = h^2/12$, $y' = 0.5$, $h = 0.00406$ ft.).

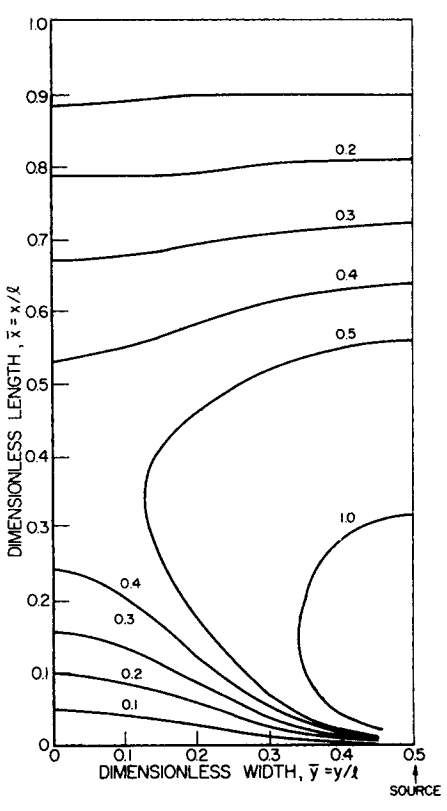

Fig. 5. Lines of constant dimensionless x direction seepage velocity q_x^0 at zero time ($\gamma = 1.0$, $k_x = k_y = h^2/12$, $y' = 0.5$, $h = 0.00406$ ft.).

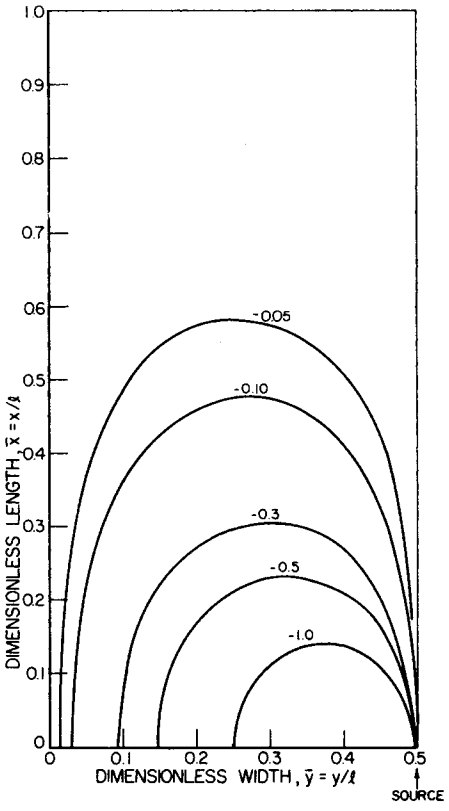

Fig. 6. Lines of constant dimensionless y direction seepage velocity, q_y^0 at zero time ($\gamma = 1.0$, $k_x = h^2/12$, $y' = 0.5$, $h = 0.00406$ ft.).

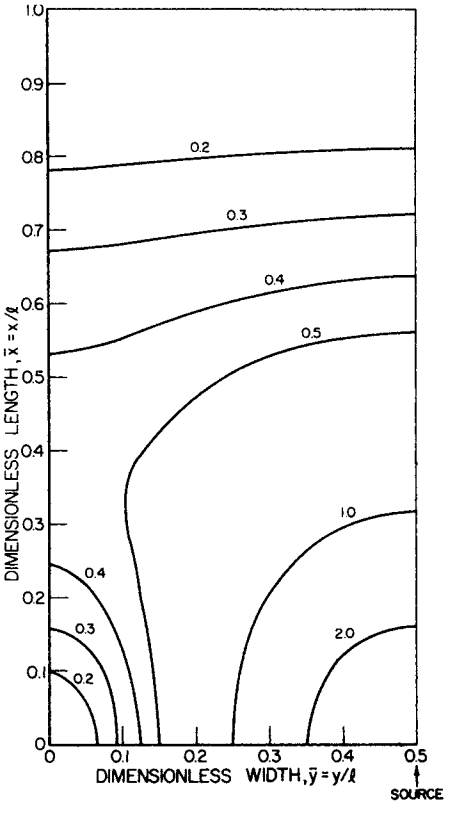

Fig. 7. Lines of constant dimensionless speed q at zero time ($\gamma = 1.0$, $k_x = k_y = h^2/12$, $y' = 0.5$, $h = 0.00406$ ft.).

of these is a verification of the satisfaction of the continuity equation in the form

$$\frac{\partial q_x}{\partial x} + \frac{\partial q_y}{\partial y} = -\frac{I}{hnFC} \tag{43}$$

for constant density. Integration of Equation (43) over an arbitrary closed region A, and use of Green's theorem in the plane, produces

$$\int_\Gamma (q_y\,dx - q_x\,dy) = \iint_A \frac{I}{hnFC}\,dA = Q_{\text{consumed}} \tag{44}$$

When the line integral indicated is used over the boundaries $y = 0$, $y = w$, $x = 0$ and any arbitrary line $x = X$, we obtain

$$-\int_0^w q_x\,dy = Q_{\text{consumed}} - Q_{\text{source}} = \left(\int_0^w \int_0^X - \int_0^w \int_0^l\right) \frac{I}{hnFC}\,dx\,dy \tag{45}$$

which may be rearranged in dimensionless form as

$$\int_0^\gamma \int_{\bar{X}}^1 \psi\,d\bar{x}\,d\bar{y} - \int_0^\gamma \bar{q}_x(\bar{X}, \bar{y})\,d\bar{y} = 0 \tag{46}$$

If there is a leak across $x = X$, the result of Equation (46) will be negative. The balance was performed for eight points inside the rectangle. It was found that the maximum error in Equation (46) was always within several tenths of a percent.

The mass balance in time may be derived by integrating the species equation over time and space and using all the boundary conditions. The result is

$$\int_0^\theta \bar{\psi}_{\text{avg}}\,d\theta = \frac{x_a^0 - x_{a_{\text{avg}}}}{1 - x_a^i} \tag{47}$$

Equation (47) relates the average concentration of the inerts in the cell to the total current drawn up to time θ. This equation was used as a check to see whether errors were accumulating as time progressed. It was satisfied quite closely (2).

COMPUTATIONAL RESULTS

The Hele-Shaw flow case represents the most two-dimensional case and shows the trends most clearly. Therefore we discuss it first. Here the porosity and permeability ratios are equal to unity as are the open area factors. All

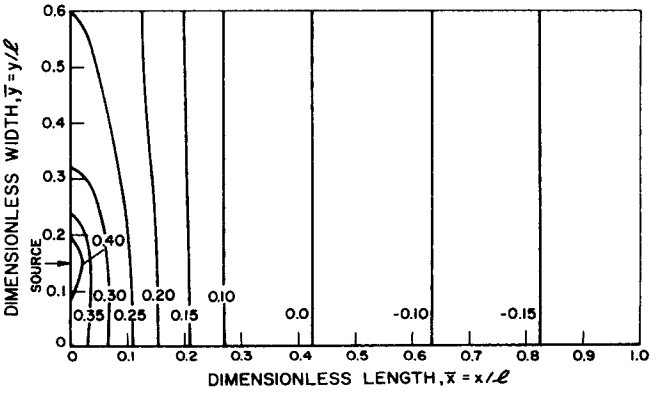

Fig. 8. Lines of constant dimensionless perturbation pressure P^0 at zero time ($\gamma = 0.6$, $k_y/k_x = 8.1$, $y' = \gamma/4$).

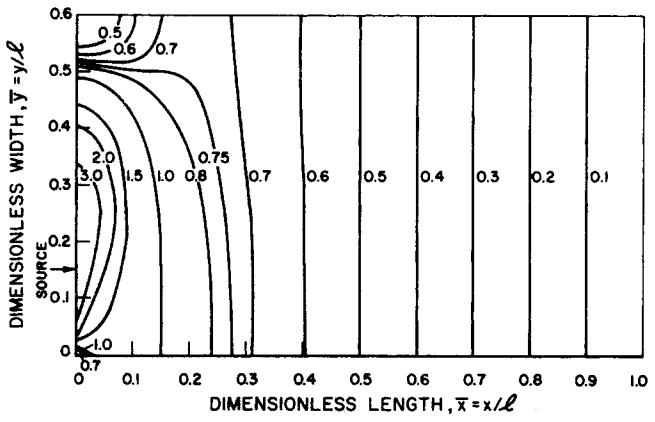

Fig. 9. Typical lines of constant speed for an Allis Chalmers dead-ended fuel cell at zero time ($\gamma = 0.6$, $k_y/k_x = 8.1$, $y' = 0.15$).

results were obtained using a Univac 1108 Mod II and an IBM 360/75 computers. These machines compare closely in running time. The computation time for the two-dimensional model is slightly lower than the experimental fuel cell operating time, using these machines.

Figure 10 shows lines of constant concentration for the inlet port opening placed at $\bar{y}' = 0.15$ for a cell chamber (1.0×0.6) dimensionless units. The inlet purity of fuel is $x_a = 0.99$. The elapsed time is approximately 14 min. The figure reveals that like the one-dimensional model the inerts are accumulating at the far (extreme right of the figure) end of the cell. However, since the inlet port is asymmetrically placed, the speed is lower in the far upper corner than in the far lower corner. Consequently, inerts build up there first. This fact is quite clearly represented in Figure 10 by an elliptical region for 0.70 mole fraction of inert in the upper right-hand corner. Fortuitously, the exit port of the fuel cell is also placed near this corner where the inert concentration is highest. Purging or bleeding at this time of 14.1 min. would initially remove inert gas of 70 mole % concentration.

Figure 11 is a plot of the inert distribution for an elapsed time of 26.5 min. The dead-ended portion of the cell is becoming more one-dimensional owing to the blanketing effect and almost complete lack of reactant. Since the velocity is practically zero here, no fresh gas can enter. The two-dimensional effect is most pronounced in the band where the concentration is changing the most rapidly. Once again, near the left hand of the graph, the concentration becomes more one-dimensional owing to the rapid flow of gases.

Realistic cases were run using the permeabilities for an Allis-Chalmers cell. The permeability ratio used is from Sareen and Gidaspow's (5) study which is for the hydrogen chamber. The oxygen chamber permeability ratio should be slightly lower since the slotting is less extensive. The results for the run are presented in Figure 12 where lines of constant mole fraction of inert are drawn. The characteristic elliptical area of inert buildup in the upper right-hand corner is again present as it was for the case of an empty chamber, however, it is both much thinner and more elongated as compared to that in Figure 10. It is also obvious that the inert distribution is almost completely one-dimensional, as evidenced by the straightness of the constant mole fraction lines.

It is now possible to make a comparison of our results with both the one-dimensional model and the one experimental run of Allis-Chalmers. This is done in Figure 13. The value of h_{eq} used for the one-dimensional model is the same used in Part I of this study (*1, 2*), and represents very nearly the height of two grooves in the direction of flow. The value of h_{av}, which is the cell's volume to surface ratio, is picked such that we compare the same cell volumes for both the one- and two-dimensional models. Since we do not know the exact conditions of the Allis-Chalmers

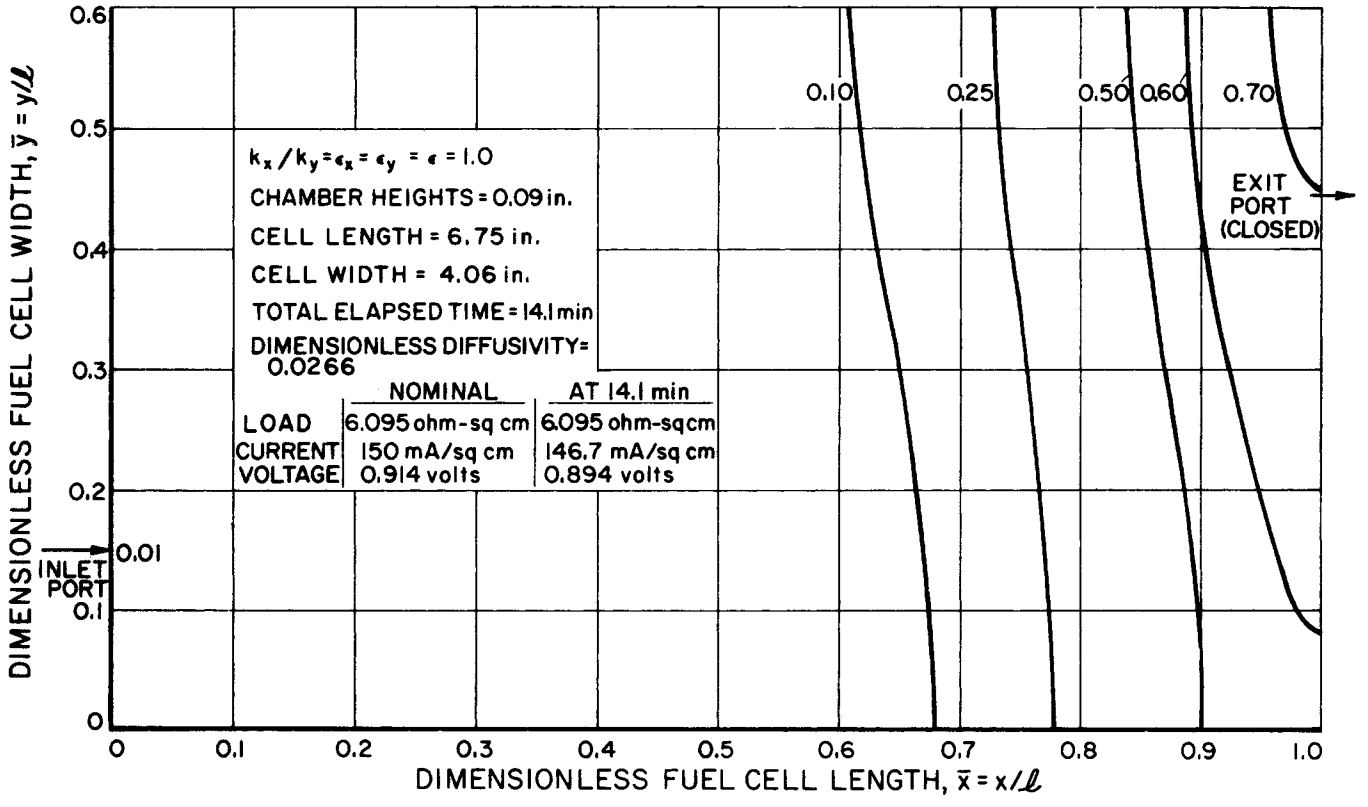

Fig. 10. Two-dimensional buildup of inerts in a dead-ended fuel cell cavity at $t = 14.1$ min.

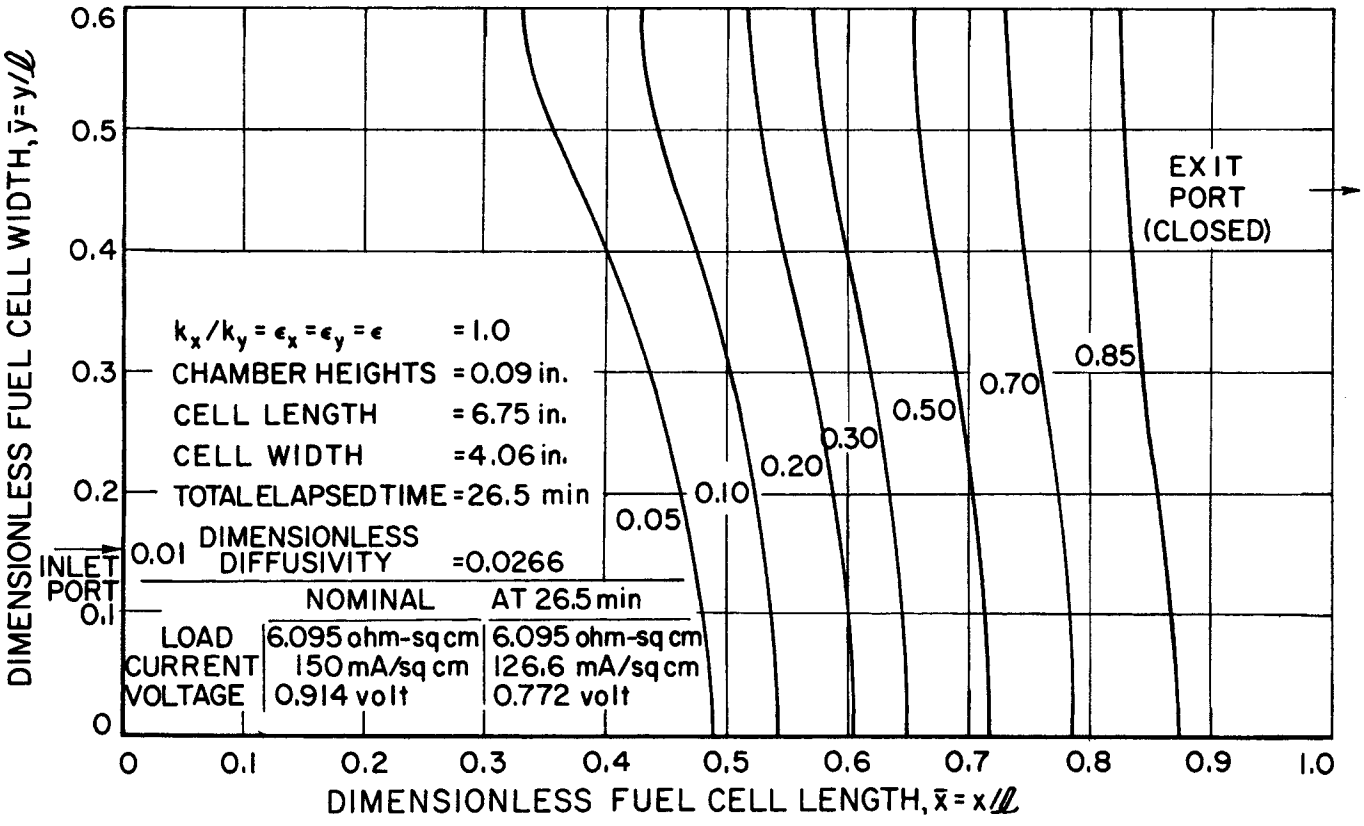

Fig. 11. Two-dimensional buildup of inerts in a dead-ended fuel cell cavity at $t = 26.5$ min.

experiment, a value of ϵ was chosen so that the two-dimensional results agree as closely as possible to the experimental average current density. This amounts to adjusting the time scale since ϵ scales the actual time.

Figure 13 shows that with a value of $\epsilon = 0.63$, the two-dimensional results fall right on the experimental curve for short times. As time progresses, the two-dimensional plot lies slightly above, and then decreases until it crosses the experimental curve; then it lies slightly below. The maximum deviation from the experimental run is ±2 mamp./sq.cm. The one-dimensional results lie below the experiment, cross at two closely spaced points, and then fall off too rapidly until they are in poor agreement for longer time. In a least squares sense, the two-dimensional model agrees better with the experimental results than do the one-dimensional results.

The amount of computer time necessary to run a typical realistic case is excessively high when low amounts of impurity are introduced. In addition, since the continuity equation is not satisfied identically, the calculations are quite sensitive in all aspects. A premature steady state condition is one manifestation of this sensitivity due to leaks, as discussed in the previous section. In light of this situation parametric studies are best done using higher impurity concentrations. A run employing realistic parameters was run with 5% inert. This high amount of impurity causes a very rapid decay in time and tends to overshadow any effects that might be caused by slight dissatisfaction of the continuity equation. Local inert concentration buildup is shown in Figure 14. The right half of the figure shows that the cell contains all inerts. Near the pin hole opening, an elliptical area exists for lower amounts of impurity. In addition, inert concentration is higher in the upper left-hand corner than in the lower left-hand corner since the speed is higher near the source. In con-

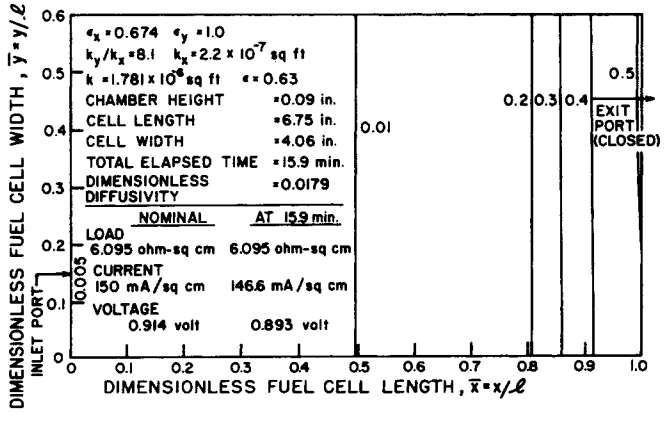

Fig. 12. Two-dimensional buildup of inerts in a typical Allis-Chalmers fuel cell at $t = 15.9$ min.

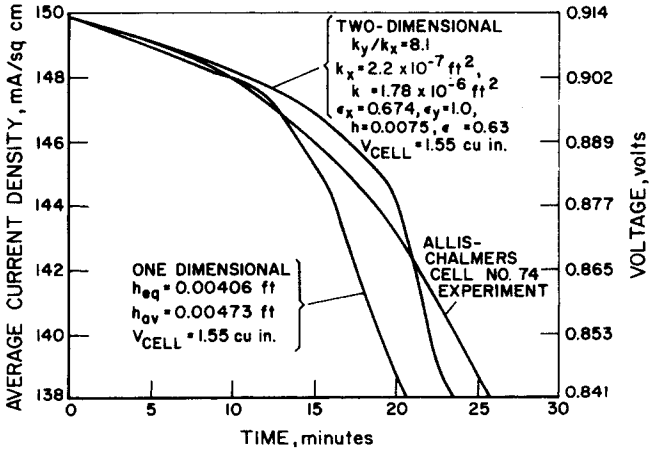

Fig. 13. Comparison of one- and two-dimensional models to Allis-Chalmers experimental results for an oxygen chamber.

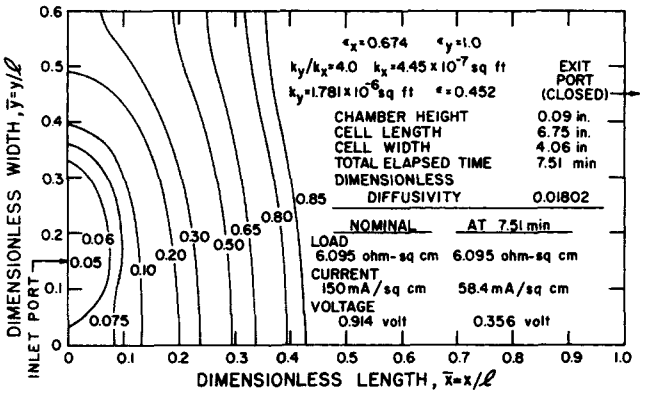

Fig. 14. Two-dimensional buildup of inerts in a dead-ended fuel cell cavity at $t = 7.51$ min; 95% pure oxygen feed.

trast to the concentration distribution for lower amounts of inert accumulation, Figure 12, two-dimensionality is much more in evidence here.

It can be concluded from this study that for realistic parameters, two-dimensionality is not in great evidence for concentration profiles with a low inert buildup and relatively small current degradation. However, when a great deal of inert is allowed to accumulate, a pronounced two-dimensional distribution results. Nonetheless, for average quantities, such as the current density, there is still quite close agreement with results produced from the one-dimensional model. For long times, the two-dimensional model begins to fall below the one-dimensional model. This trend is in the correct direction since the one-dimensional model begins to lie above the experimental curve (*1, 2*). The average current density produced from the two-dimensional model would lie closer to an experimental curve than average current density produced from the one-dimensional model for longer times.

To assess the effect of permeability ratio, another run was made with a different value of this parameter. The results are shown in reference 2. In general, changing the permeability ratio has little effect. Increasing this ratio does make the average current density resemble one-dimensional results more closely. For shorter times, a higher permeability ratio makes results lower, and for longer times, it makes the current density increase. Both of these tendencies make the two-dimensional results resemble one-dimensionality more closely.

It should be pointed out that the rectangular geometry is only a special case. Once the Green's function for the Neumann problem is obtained, the solution for the geometry under consideration is, in principle, available, as shown in this paper. For example, the fuel cell problem with distributors near the inlet and the outlet leads to a three-region composite media problem for which the Green's functions were recently constructed (*14*).

ACKNOWLEDGMENT

This study was supported by the National Aeronautics and Space Administration under Contract No. NAS 8-21159 and IGT Basic Research funds. The authors are grateful to Richard Boehme of the NASA Marshall Space Flight Center for suggesting this problem. They also thank B. S. Baker, D. Y. C. Ng, C. W. Solbrig, W. Toczycki, and G. von Behren for their various services without which this work could not have been carried out, and Charles Tobias for useful and stimulating discussion of this problem.

NOTATION

a = species a reactant gas; $(k_x/k_y)^{1/2}\,\pi/\gamma$
b = π/γ; species b
C = total molar concentration, lb.-moles/cu.ft.
C_a = molar concentration of species a, lb.-moles/cu.ft.
D^* = dimensionless diffusivity = $\epsilon_x D_{ab} hnFC/l^2 I_0$
D_{ab} = binary diffusivity of reactant gas a in inert gas b, sq.ft./hr.
F = Faraday's constant, 12,158 amp.-hr./lb.-equivalent
G = Green's function
g_c = gravity conversion factor, 32.2 $(\text{lb.}_m/\text{lb.}_f)$ (ft./sec.^{2})
h = height of fuel cell cavity, ft.
I = current density, amp./sq.ft.
I_0 = average current density at zero time, amp./sq.ft.
k_x, k_y = permeabilities in Darcy's law
l = length of fuel cell cavity, ft.
M_a, M_b = molecular weights of species a and b
n = number of lb.-equivalents per lb.-mole (= 4 for oxygen)
P = cavity pressure, lb._f/sq.ft.
$\bar{P}$ = perturbation pressure, ratio of pressure to viscous forces
$= Pg_c hnFCk_x/l^2 I_0 \mu$
$\bar{q}$ = dimensionless speed = $\sqrt{(\bar{q}_x)^2 + (\bar{q}_y)^2}$
q_x, q_y = molar average seepage velocities in the x and y directions
q_x^*, q_y^* = weight average seepage velocities in the x and y directions
$\bar{q}_x$, $\bar{q}_y$ = dimensionless seepage velocities = $q_{x,y} \Big/ \left(\frac{I_0\, l}{hnFC}\right)$
Q = dimensionless flow as defined by Equation (27)
t = time, hr.
v_a = velocity of species a, ft./sec.
v_x, v_y = mass average velocity components in the x and y directions, $= (\rho_a v_{a_{x,y}} + \rho_b v_{b_{x,y}})/\rho$, ft./hr.
w = width of fuel cell cavity, cm.
x = space coordinate in the main direction of flow, ft.
$\bar{x}$, $\bar{y}$ = dimensionless space coordinates, x/l, y/l
x_a = mole fractions of species a
y = space coordinate, ft.
(x', y') = source coordinates
(x'', y'') = sink coordinates

Greek Letters

γ = aspect ratio = w/l
$\bullet$ = ratio of actual volume to nominal volume of fuel cell chamber
ϵ_x, ϵ_y = ratios of actual to open area in the x and y directions
θ = dimensionless time = $t\, I_0/hnFC\epsilon$
μ = system viscosity, lb./(ft.)(hr.)
ρ = total system density, lb./cu.ft.
ρ_a = mass concentrations of species a, lb./cu.ft.
ψ = dimensionless current density, I/I_0

LITERATURE CITED

1. Lyczkowski, R. W., and Dimitri Gidaspow, *AIChE J.*, **17**, 1208 (1971). Paper presented at AIChE Washington, D. C. meeting (1969).
2. Lyczkowski, R. W., Ph.D. thesis, Illinois Inst. Technol., Chicago (1970).
3. Gidaspow, Dimitri, and S. S. Sareen, *AIChE J.*, **16**, 560-568 (1970).
4. ———, *Proc. 4th Meeting Intersoc. Energy Conversion Eng. Conf.*, 920-32 (1969).
5. Inst. Gas Technol., *Final Rept., Contract No. NAS 8-21159* for George C. Marshall Space Flight Center, NASA Huntsville, Ala., Chicago, Oct., 1969 (NAS 8-21159-SR-002).
6. Lee, R. G., and T. E. Weber, *Can. J. Chem. Eng.*, **47**, 54-59 (1969).

7. Schlichting, H., "Boundary Layer Theory," 4th edit., McGraw-Hill, New York (1960).
8. Carslaw, H. S., and J. C. Jaeger, "Conduction of Heat in Solids," 2nd edit., Oxford Univ. Press (1959).
9. Keller, H. B., in "Mathematical Methods for Digital Computers," A. Ralston and H. S. Wilf, eds., Chap. 12, Wiley, New York (1960).
10. Abramowitz, Milton, and I. A. Stegun, *NBS Appl. Math Ser. No. 55*, Govt. Printing Office, Washington, D. C. (1964).
11. Allis-Chalmers Res. Div., *Summary Rept. Contract No. NAS 8-5392* for George C. Marshall Space Flight Center, NASA, Huntsville, Ala., Milwaukee, Jan. 15, 1966 (NAS 8-5392-SR-0001).
12. Bauche, Wilhelm, and August Winsel, *Advanced Energy Conversion*, 3, 661-645 (1963).
13. Winsel, August, *Electrochimica Acta*, **14**, 961-970 (1969).
14. Sareen, S. S., Ph.D. thesis, Illinois Inst. Technol., Chicago (1970).

APPENDIX

The final expression for pressure used in this study is shown in this section. It is obtained in the same manner as for $\theta = 0$ by substituting Equation (30) into Equation (26). In this case, however, the double integral over the entire rectangle is replaced by a double sum of integrals, each integrated over the smaller rectangle. When all the integrations are performed and the terms grouped, the solution for the pressure assumes the form given below. We call the reader's attention to the variable ξ which had to be introduced to keep track of the inequalities arising out of the single series representation of the Green's function given by Equation (29), and the use of the expression for P outside the range of the small rectangle within the fuel cell.

$$P(x, y; 0, y') = \frac{Q}{\gamma} P^0(x, y; 0, y')$$

$$- \sum_{i}^{MX} \sum_{j}^{NY} \frac{\Delta y'}{\gamma} \left[A^{ij} + C^{ij} \left(y_{j-1} + \frac{\Delta y'}{2} \right) \right]$$

$$\left\{ \frac{1}{2} \left[(x^2 (\xi - x_{i-1}) \right.\right.$$

$$+ \frac{1}{3} (\xi^3 - x^3{}_{i-1}) \Big] - x(\xi - x_{i-1}) + \frac{1}{3} (\xi - x_{i-1})$$

$$+ \frac{1}{2} \left[x^2(x_i - \xi) + \frac{1}{3} (x_i{}^3 - \xi^3) \right]$$

$$\left. - \frac{1}{2} (x_i{}^2 - \xi^2) (x_i - \xi) \right\}$$

$$+ \frac{\Delta y}{\gamma} \left[B^{ij} + D^{ij} \left(y_{j-1} + \frac{\Delta y'}{2} \right) \right]$$

$$\left\{ \frac{1}{2} \left[\frac{x^2}{2} (\xi^2 - x^2{}_{i-1}) \right.\right.$$

$$+ \frac{1}{4} (\xi^4 - x^4{}_{i-1}) \Big] - \frac{x}{2} (\xi^2 - x^2{}_{i-1}) + \frac{1}{6} (\xi^2 - x^2{}_{i-1})$$

$$+ \frac{1}{2} \left[\frac{x^2}{2} (x_i{}^2 - \xi^2) + \frac{1}{4} (x_i{}^4 - \xi^4) \right]$$

$$\left. - \frac{1}{3} (x_i{}^3 - \xi^3) + \frac{1}{6} (x_i{}^2 - \xi^2) \right\}$$

$$+ \frac{8\pi^2}{a^2} A^{ij} \sum_{1}^{\infty} \cos(mby) \cdot I \cdot \{G \cosh [am(1 - x)]$$

$$- H \cosh(amx)\}/[(m\pi)^3 \sinh(am)]$$

$$+ \frac{4\pi}{a} B^{ij} \sum_{1}^{\infty} \cos(mby) \cdot I \cdot \{C \cosh [am(1 - x)]$$

$$+ E \cosh (amx)\}/[(m\pi)^3 \sinh(am)]$$

$$- \frac{8\pi^3}{a^3} B^{ij} \sum_{1}^{\infty} \cos (mby) \cdot I \cdot \{D \cosh [am(1 - x)]$$

$$+ F \cosh (amx)\}/[(m\pi)^2 \sinh(am)]$$

$$+ \frac{4\pi^2}{a^2} C^{ij} \sum_{1}^{\infty} \cos (mby) \cdot A \cdot \{G \cosh [am(1 - x)]$$

$$- H \cosh (amx)\}/[(m\pi)^3 \sinh(am)]$$

$$- \frac{8\gamma\pi^2}{a^2} C^{ij} \sum_{1}^{\infty} \cos (mby) \cdot B \cdot \{G \cosh [am(1 - x)]$$

$$- H \cosh (amx)\}/[(m\pi)^4 \sinh(am)]$$

$$+ \frac{2\pi^2}{a^2} D^{ij} \sum_{1}^{\infty} \cos (mby) \cdot A \cdot \{C \cdot \cosh [am(1 - x)]$$

$$+ D \cosh (amx)\}/[(m\pi)^3 \sinh(am)]$$

$$- \frac{4\pi^2}{a^2} D^{ij} \sum_{1}^{\infty} \cos (mby) \cdot \left\{ B\gamma(C \cdot \cosh [am(1 - x)] \right.$$

$$+ D \cosh (amx)) + \frac{\pi A}{a} (D \cosh [am(1 - x)$$

$$\left. + F \cosh (amx)) \right\} \Big/ [(m\pi)^4 \sinh(am)]$$

$$+ \frac{8\gamma\pi^3}{a^3} D^{ij} \sum_{1}^{\infty} \cos (mby) \cdot B \{D \cosh [am(1 - x)]$$

$$+ F \cosh amx\}/[(m\pi)^5 \sinh(am)]$$

where, ad hoc

$$A = y_j \sin(mby_j) - y_{j-1} \sin(mby_{j-1})$$

$$B = \sin \left[\frac{mb(y_j + y_{j-1})}{2} \right] \sin \left(\frac{mb\, \Delta y'}{2} \right)$$

$$C = \xi \sinh (am\, \xi) - x_{i-1} \sinh (amx_{i-1})$$

$$D = \sinh \left[\frac{am(\xi + x_{i-1})}{2} \right] \sinh \left[\frac{am(\xi - x_{i-1})}{2} \right]$$

$$E = \xi \sinh [am(1 - \xi)] - x_i \sinh [am(1 - x_i)]$$

$$F = \sinh \left[\frac{am(2 - (\xi + x_i))}{2} \right] \sinh \left[\frac{am(\xi - x_i)}{2} \right]$$

$$G = \cosh \left[\frac{am(\xi + x_{i-1})}{2} \right] \sinh \left[\frac{am(\xi - x_{i-1})}{2} \right]$$

$$H = \cosh \left[\frac{am(1 - \tfrac{1}{2}(x_i + \xi))}{2} \right] \sinh \left[\frac{am(\xi - x_i)}{2} \right]$$

$$I = \cos \left[\frac{mb(2y_{j-1} + \Delta y')}{2} \right] \sin \left(\frac{mb\, \Delta y'}{2} \right)$$

and

$$Q = \Delta x' \Delta y' \sum_{i=1}^{MX} \sum_{j=1}^{NY} A^{ij} + B^{ij} \left(x_{i-1} + \frac{\Delta x'}{2} \right)$$

$$+ C^{ij} \left(y_{j-1} + \frac{\Delta y'}{2} \right) + D^{ij} \left(x_{i-1} + \frac{\Delta x'}{2} \right) \left(y_{j-1} + \frac{\Delta y'}{2} \right)$$

where

$$\xi = \begin{cases} x_i & \text{if } x > x_i \\ x_{i-1} & \text{if } x < x_{i-1} \\ x & \text{if } x_i \geqq x \geqq x_{i-1} \end{cases}$$

Manuscript received January 20, 1970; revision received August 20, 1970, paper accepted August 24, 1970.